Unified approach to electronic, thermodynamical, and transport properties of Fe_3Si and Fe_3Al alloys

J. Kudrnovský and V. Drchal
Institute of Physics, Academy of Sciences of the Czech Republic, CZ-182 21 Praha 8, Czech Republic

L. Bergqvist
Dept. of Materials and Nanophysics and Swedish e-Science Research Centre (SeRC), KTH Royal Institute of Technology, Electrum 229, S-164 40 Kista, Sweden

J. Rusz
Department of Physics and Astronomy, Uppsala University, Box 516, S-751 20 Uppsala, Sweden

I. Turek
Faculty of Mathematics and Physics, Department of Condensed Matter Physics, Charles University, Ke Karlovu 5, CZ-12116 Praha 2, Czech Republic

B. Újfalussy and I. Vincze
Wigner Research Centre for Physics, Hungarian Academy of Sciences, Konkoly-Thege M. út 29-33., H-1121 Budapest, Hungary
(Received 18 July 2014; revised manuscript received 15 September 2014; published 10 October 2014)

The electronic, thermodynamical, and transport properties of ordered Fe_3X (X = Al,Si) alloys are studied from first principles. We present here a unified approach to the phase stability, the estimate of the Curie temperature, the temperature dependence of sublattice magnetizations, magnon spectra, the spin-stiffnesses, and residual resistivities. An important feature of the present study is that all calculated physical properties are determined in the framework of the same first-principles electronic structure model combined with the effective Ising and Heisenberg Hamiltonians used for study of the thermodynamical properties of alloys. Curie temperatures, spin-stiffnesses, and magnon spectra are determined using the same calculated exchange integrals. Finally, the transport properties are calculated using the linear-response theory. Our theoretical estimates compare well with available experimental data. In particular, calculations predict (in agreement with experiment) the ordered $D0_3$ phase as the ground-state alloy structure, demonstrate that a correct relation of Curie temperatures of Fe_3Al/Fe_3Si alloys can be obtained only by going beyond a simple mean-field approximation, provide reasonable estimates of spin-stiffnesses, and give resistivities compatible with structural disorder observed in the experiment. Although the calculated temperature dependences of the Fe magnetization on different sublattices are similar, they nevertheless deviate more than in the experiment, and we discuss a possible origin.

DOI: 10.1103/PhysRevB.90.134408 PACS number(s): 64.60.Ej, 71.15.−m, 72.15.−v, 75.10.Hk

I. INTRODUCTION

Iron-rich metal alloys are interesting materials for various technological applications. Among these alloys, those containing *sp* metals such as aluminum and silicon have, in addition, high strength and resistance to oxidation. Regarding their magnetic properties, one can mention the high magnetic permeability and large magnetostriction. Specifically, at around 25% of the *sp* element, they form ordered Fe_3Al and Fe_3Si compounds crystallizing in the $D0_3$ structure, which is formed by four fcc sublattices A-B-C-D along the [111] direction with the order Fe[A]-Fe[B]-Fe[C]-X[D], X = Al,Si.

In Fe_3Al, the high-temperature disordered body-centered-cubic structure after cooling orders first into the B2 (CsCl-type) structure, and, after further cooling, it orders into the $D0_3$ structure. Stoichiometric Fe_3Si exhibits $D0_3$ order up to very high temperatures (1500 K). We refer the reader to Ref. [1] for a detailed experimental account of the phase diagrams. Another interesting feature of these materials is related to the fact that two kinds of iron sites exist: the first type—containing Fe[B] atoms—with its nearest neighbors being only iron atoms as in bcc Fe, and the other type—comprised of Fe[A] and Fe[C] atoms—which have as nearest neighbors both iron and *sp*-metal atoms. As a result, the transition-metal impurities show a selective preference site occupation on the above two types of sublattices [2]. At higher impurity concentrations, these alloys have a direct relation to the Heusler-type alloys with the $L2_1$ structure. The above-mentioned two types of sites exhibit also very different magnetic behavior under an external pressure. While the bcc-type site behaves similarly to bcc Fe, the other two exhibit an interesting metamagnetic behavior close to the equilibrium volume [3,4].

The electronic structure and ground-state properties of these materials were studied intensively in the past using first-principles approaches. We therefore mention just two early studies, namely Refs. [5] and [6] for Fe_3Al and Fe_3Si, respectively. On the other hand, a number of interesting properties, such as, e.g., the order-disorder phase transition, exchange integrals, Curie temperatures, magnetization thermodynamics, or transport properties, have not yet been studied systematically, in particular not on the first-principles theory level. The main feature that distinguishes the present paper from a number of related studies of these and similar alloys is that we evaluate a large number of physically different quantities, such as the Curie temperature, residual resistivity, magnetic moments, spin stiffness, the phase stability,

and magnon dynamics using the same electronic structure model, rather than evaluating them using different individually tailored inputs. Conventionally, just a few closely related quantities, such as, e.g., the band structure and densities of states, equilibrium volume, etc., are presented. Without estimation of other, physically different quantities within a given approach, one obtains only an incomplete understanding. As a byproduct, we also estimate physical properties that were not evaluated to date from first-principles. The above alloys represent a suitable object for such a project because a lot of reliable experimental data were gathered in the past that are missing for many recently prepared materials.

The following problems are addressed: (i) the study of ordering from the disordered bcc phase into the $D0_3$ structure for Fe_3Al and Fe_3Si using an alloy Ising model constructed from first principles and clarifying the role of magnetic moments in the order-disorder transition; (ii) evaluation of exchange integrals and construction of a corresponding classical Heisenberg Hamiltonian, which can be used to estimate the Curie temperature of Fe_3Al and Fe_3Si, in particular to explain the larger Curie temperature of Fe_3Si, and to determine the magnon spectra; (iii) the thermodynamic study of sublattice magnetizations, motivated by the fact that the measured sublattice-resolved Fe hyperfine fields behave very similarly [7] despite their different local environment (bcc-like for the Fe[B] sublattice and mixed iron and sp metal for the Fe[A,C] sublattices). Since the hyperfine fields are not the main subject of this study, a simple model relating the sublattice magnetizations and the hyperfine fields is presented in the Appendix; (iv) the low-temperature transport properties, in particular the role played by native disorder that causes the finite resistivity of stoichiometric compounds. All results are compared with the available experimental data.

II. FORMALISM AND COMPUTATIONAL DETAILS

The electronic structure calculations were performed using the scalar-relativistic tight-binding linear muffin-tin orbital (TB-LMTO) scheme [8] within the local density approximation (LDA). The Vosko-Wilk-Nusair exchange-correlation potential [9] was used for the parametrization of the local density functional. A possible effect of disorder (e.g., disordered bcc phase used for study of phase transformations or the use of native disorder in transport calculations) is described by the coherent-potential approximation (CPA) as formulated in the framework of the TB-LMTO Green's function method [10]. The same atomic sphere radii were used for all constituent atoms, lattice constants were taken from the experiment, and the s,p,d,f basis was used in all calculations.

The phase stability of the alloy A_xB_{1-x} is described by the Ising alloy Hamiltonian

$$H^{\mathrm{I}} = \sum_{i \neq j} V_{ij} \eta_i \eta_j, \tag{1}$$

where i,j are site indices and η_i is the occupation index, which is 1 if the site i is occupied by atom A and 0 otherwise. The quantities V_{ij} are the effective interatomic (chemical) interactions. The chemical interactions V_{ij} are determined using the generalized perturbation method (GPM) of Ducastelle [11]. Their determination within the TB-LMTO is described in Ref. [12]. It should be noted that V_{ij} depend on the presence of magnetic moments [12]. The positive/negative values of effective pair interactions indicate the tendency to prefer unequal/similar atom pairs in the alloy. It should be noted that the GPM method derives chemical interactions from the reference disordered system without assuming any ordered structure. Possible ordered phases are then obtained on the basis of thermodynamics either using the Monte Carlo approach or simpler mean-field approaches, the concentration-wave method in the present case [11]. It should be noted that the Ising alloy Hamiltonian can also be constructed assuming a set of possible ordered structures using the so-called Connolly-Williams approach [13].

The magnetic structure is described by the classical Heisenberg Hamiltonian

$$H^{\mathrm{H}} = -\sum_{i \neq j} J_{ij} \mathbf{e}_i \cdot \mathbf{e}_j. \tag{2}$$

Here i,j are again site indices, $\mathbf{e}_i$ is the unit vector in the direction of the local magnetic moment at site i, and the quantities J_{ij} are exchange integrals between sites i and j. The exchange integrals J_{ij} are determined using the method of infinitesimal rotations of Liechtenstein [14]; its implementation within the TB-LMTO method can be found in Ref. [15]. The exchange integrals, by construction, contain magnetic moments of atoms; their positive (negative) values indicate a tendency to ferromagnetic (antiferromagnetic) coupling.

The Curie temperatures can be estimated from calculated exchange interactions using the mean-field approximation (MFA),

$$k_B T_c^{\mathrm{MFA}} = \frac{2}{3} \sum_{i \neq 0} J_{0i}, \tag{3}$$

and the random-phase approximation (RPA) [16],

$$\left(k_B T_c^{\mathrm{RPA}}\right)^{-1} = \frac{3}{2} \frac{1}{N} \sum_{\mathbf{q}} [J(\mathbf{0}) - J(\mathbf{q})]^{-1}, \tag{4}$$

where $J(\mathbf{q})$ is the lattice Fourier transform of J_{ij}'s. For multisublattice versions of these formulas, we refer the reader to Ref. [17].

The residual resistivities are determined by the linear-response theory as formulated in the framework of the TB-LMTO-CPA method using the Kubo-Greenwood (KG) formula [18] including the disorder-induced vertex corrections [19]. Such vertex corrections are equivalent to the backward scattering in the collision term of the Boltzmann transport theory. The relevance of vertex corrections depends on the specific alloy and should be checked for each system. Their importance for calculated resistivities was demonstrated in Ref. [20]. We refer the readers to Refs. [18,19] for details concerning the formulation of transport theory.

III. RESULTS AND DISCUSSION

In this section, we present theoretical estimates of various physical quantities related to Fe_3Al and Fe_3Si.

TABLE I. Calculated local magnetic moments (th) of Fe atoms on the A/C and B sites are compared with available experimental data obtained from the neutron measurements done at room temperature (RT). We also show values extrapolated down to the zero (0) temperature [22], which are the most suitable for comparison with theoretical results.

	Local magnetic moments in μ_B					
Alloy	$M^{Fe}_{A,C}$(RT)	M^{Fe}_{B}(RT)	$M^{Fe}_{A,C}$(0)	M^{Fe}_{B}(0)	$M^{Fe}_{A,C}$(th)	M^{Fe}_{B}(th)
Fe_3Si [23]	1.07 ± 0.06	2.23 ± 0.06	1.15	2.40	1.24	2.53
Fe_3Si [24]	1.20 ± 0.12	2.40 ± 0.06	1.29	2.58	1.24	2.53
Fe_3Al [25]	1.50 ± 0.10	2.18 ± 0.10	1.66	2.41	1.79	2.35

A. Local magnetic moments

The Fe[B] moment with the bcc-type environment is large, being of order $2.5\mu_B$, while the Fe[A] and Fe[C] moments (the same by symmetry) are much smaller. Even more important is the fact that while the Fe[B] moment is rigid with respect to spin rotations, the Fe[A,C] moments are not. More specifically, while in the ferromagnetic and in the disordered local moment (DLM) [21] states the moments on the Fe[B] sites are similar, the Fe[A,C] moments collapse to zero in the DLM.

We have summarized the calculated and experimental values of local moments $M^{Fe}_{A,C}$ and M^{Fe}_{B} in Table I. We find a reasonable agreement of calculated and experimental values, in particular for those extrapolated to zero temperature. Our results also agree with other theoretical calculations for Fe_3Al, Ref. [26], and Fe_3Si, Ref. [27]. Calculated local moments on sp-metal atoms are small and negative, being $-0.07\mu_B$ and $-0.11\mu_B$ for Fe_3Si and Fe_3Al, respectively.

For completeness, we also mention the calculated DLM moments of ordered compounds: $M^{Fe}_{B} = \pm\ 2.68\ (\pm 2.51)\mu_B$ for Fe_3Si (Fe_3Al), respectively while $M^{Fe}_{A,C}$ moments (and sp moments on Al and Si) are zero.

B. Alloy phase stability

We illustrate the present approach in detail on the determination of the alloy phase stability of the Fe_3Al alloy. First, it is well known [11] that the bcc lattice cannot order directly into the $D0_3$ phase. Experimentally [28], the completely disordered high-temperature (A2) phase (or bcc-$Fe_{75}Al_{25}$ alloy) after cooling exhibits the first phase transition into the ordered B2 phase at around 1020 K [CsCl-type, the sublattice order is Fe-(Fe_{50},Al_{50})-Fe-(Fe_{50},Al_{50})]. After further cooling to 820 K, the secondary transition from the B2 phase into the $D0_3$ phase occurs.

We have used as a reference state for estimation of the effective pair interaction the disordered bcc-$Fe_{75}Al_{25}$ alloy both in nonmagnetic (with zero atomic magnetic moments) and ferromagnetic states to see the possible effect of magnetic moments on the ordering [12]. The lattice Fourier transform $V(\mathbf{q})$ of V_{ij} allows us to discuss the phase stability using the method of the concentration waves [11,12]. The minimum of $V(\mathbf{q})$ at the high-symmetry point $\mathbf{q}^{ord}$ indicates an ordering tendency to form a superstructure compatible with it [11] while the minimum at $\mathbf{q}^{ord} = 0$ corresponds to a segregation of alloy components. An effective-medium order-disorder temperature in a random alloy $A_{1-x}B_x$ is $T^{ord} = -x(1-x)V(\mathbf{q}^{ord})/k_B$ [12]. We have found $\mathbf{q}^{ord} = 2\pi(1,0,0)/a$ (a is the bcc lattice parameter), which corresponds to the B2-type ordering [11] for both nonmagnetic and ferromagnetic bcc-$Fe_{75}Al_{25}$ alloys, in qualitative agreement with the experiment. As expected, the effective-medium $T^{ord} = 1796$ K for the ferromagnetic reference state is overestimated, but in better agreement with the experiment as compared to $T^{ord} = 7815$ K obtained for the nonmagnetic reference state. We have then, starting from the B2-type nonmagnetic and ferromagnetic alloy Fe-(Fe_{50},Al_{50})-Fe-(Fe_{50},Al_{50}) in the original extended structure, calculated new effective pair interactions and $V(\mathbf{q})$ on the corresponding disordered simple cubic lattice. The segregation was obtained for the nonmagnetic case ($\mathbf{q}^{ord} = \mathbf{0}$) while $\mathbf{q}^{ord} = 2\pi(1/2,1/2,1/2)/a$ was obtained in the ferromagnetic case, which corresponds to the $D0_3$ lattice in an extended four-sublattice structure. The estimated $T^{ord} = 1502$ K is again overestimated, but in qualitative agreement with experiment, i.e., T^{ord} for the $D0_3$ ordering is smaller than T^{ord} for B2 ordering. This is a simple but nontrivial result.

The Fe_3Si alloy has a stronger tendency to ordering than the Fe_3Al alloy. This can be understood from comparisons of total energies and chemical interactions V_{ij}. We first calculate the differences

$$\Delta(X,x,y) = E_{tot}[(Fe_{1-x}X_x)(Fe_{1-y}X_y)(Fe_{1-x}X_x)(X_{1-2x-y}Fe_{2x+y})] - E_{tot}[Fe_3X], \quad (5)$$

where X = Al or Si and $2x + y = 0.06$. The first term on the right-hand side of Eq. (5) denotes the total energy of randomly occupied four sublattices A-B-C-D, respectively, with indicated compositions, and the second term denotes the total energy of perfectly ordered Fe_3X alloys. We obtain Δ(Al,0.03,0) = 5.6 mRy, Δ(Al,0,0.06) = 4.3 mRy, but Δ(Si,0.03,0) = 13.9 mRy, Δ(Si,0,0.06) = 6.2 mRy, which shows a stronger tendency for ordering in the Fe_3Si alloy. This is in agreement with the values of interatomic interactions V_{ij} between the first and second neighbors calculated for disordered alloys $Fe_{75}X_{25}$: $V_1^{Al} = 13$ mRy, $V_2^{Al} = 7$ mRy, $V_1^{Si} = 32$ mRy, and $V_2^{Si} = 9$ mRy. On a qualitative level, this is not surprising in view of the expected tendency of Si atoms to form covalent bonds, in contrast with Al atoms that form metallic bonds that are less sensitive to their neighborhood. Moreover, it is also seen (both from the total energies and from pair interactions) that the transfer of X atoms from their original sublattice to the nearest-neighbor sublattice requires higher energy than the transfer to the second-neighbor sublattice.

We conclude this section by giving T^{ord} for the formation of the $D0_3$-Fe_3Si phase. Using the same approach as for Fe_3Al above, we have obtained $T^{ord} = 3185$ K, which has to be compared to the experimental value of about 1500 K. Again,

the calculated value is overestimated, being for both Fe_3Al and Fe_3Si about two times larger as compared to the experiment.

There are two reasons for the overestimation of T^{ord} values: (i) An approximate determination of chemical interactions, which neglect charge screening effects. This problem can be formally solved by using the screened Coulomb interactions [29] instead of conventional ones used here. (ii) The mean-field concentration-wave approach is known to overestimate critical temperatures. The use of the Monte Carlo or cluster-variation approaches can solve this problem [11]. Such study is, however, beyond the scope of the present paper. Summarizing, the present approach correctly describes a two-step ordering from the disordered bcc phase into the ordered $D0_3$ lattice. Despite the fact that T^{ord} temperatures are overestimated, the theory predicts, in agreement with the experiment, much larger T^{ord} for Fe_3Si as compared to Fe_3Al.

C. Exchange integrals

The calculated exchange interactions for the $D0_3$ Fe_3Al and Fe_3Si ordered alloys are shown in Figs. 1 and 2. There are four different interactions among Fe sites, namely J[A,A] = J[C,C], J[B,B], J[B,A] = J[B,C], and J[A,C]. The interactions on fcc sublattices, namely J[A,A] = J[C,C] and J[B,B], are small as they correspond to the fcc lattices with relatively large distances (the shortest distance is $0.707a$, where a is the lattice constant). The dominating interactions are those between different sublattices: J[B,A] = J[B,C] types with the shortest intersite distance ($0.433a$), and also J[A,C] interactions with the second shortest intersite distance ($0.5a$). The interactions are rather similar for both alloys, but we shall see below that their small differences are important for estimation of their Curie temperatures. These results also agree qualitatively with a model of Stearns [7] based on a fit to the experiment. In her study, just one effective value for sublattice interactions of each type is given, her D sublattice is our B one, and interactions J[A,A] and J[A,C] form a single effective interaction (see Table II in Ref. [7]). It may be interesting to compare exchange integrals of bcc Fe calculated for the lattice constant of, e.g., Fe_3Si. We have determined them in the $D0_3$ lattice with the sublattice order Fe[A]-Fe[B]-Fe[C]-Fe[D]. Results are shown

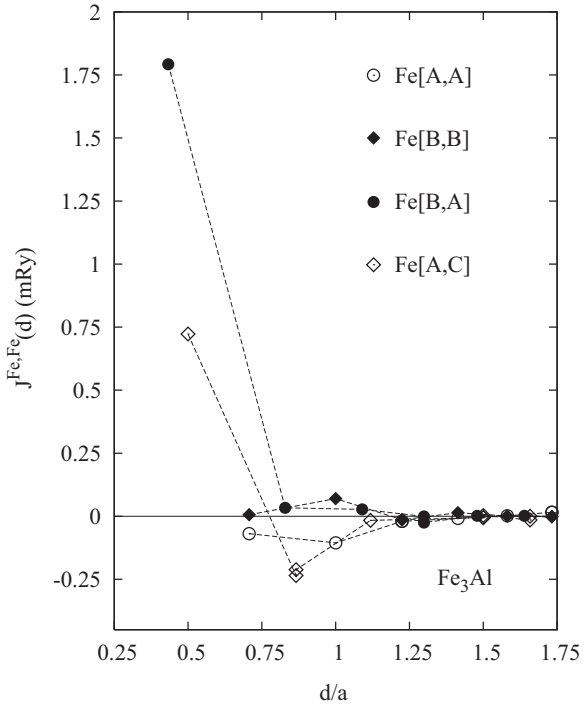

FIG. 1. The sublattice-resolved exchange interactions among various Fe sites for the ordered Fe_3Al alloy on the $D0_3$ lattice as a function of the distance (d) in units of the lattice constant (a). Four fcc sublattices along the [111] direction have the structural formula Fe[A]-Fe[B]-Fe[C]-Al[D]. Very small interactions involving Al sites are not shown.

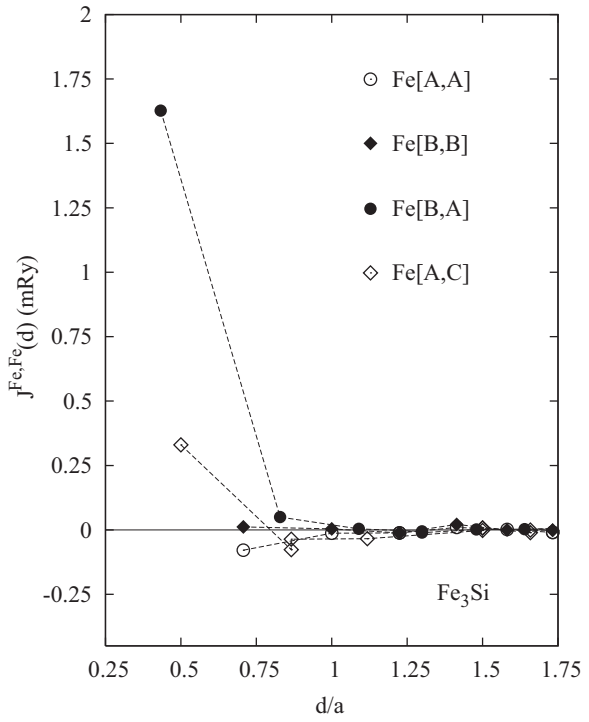

FIG. 2. The same as in Fig. 1, but for the ordered Fe_3Si alloy.

TABLE II. Calculated Curie temperatures (in K) for Fe_3X, X = Si,Al alloys in the $D0_3$ structure: the MFA, RPA, MC, and renormalized RPA approximations were tested. The experimental values 800 K [1], 830 K [46], 840 K [43], and 853 K [7] for Fe_3Si, and 713 K [7,43] and 745 K [1] for Fe_3Al, can be found in the literature. The RPA values fluctuate as a function of the number of shells of exchange integrals included in simulations (see the text for details), which is reflected by the error bars. The MC values were determined for the cutoff radii of $4a$ and $2a$ (in brackets), where a is the lattice constant. Also shown are corresponding theoretical estimates for a completely disordered bcc-$Fe_{75}Al_{25}$ alloy. The experimental Curie temperature is around 825 K [1].

		Curie temperatures			
Alloy	MFA	RPA	MC	rRPA	Expt.
Fe_3Si	1062	691 ± 1	732 (741)	920	800–853
Fe_3Al	1178	615 ± 25	695 (662)	740	713–745
$Fe_{75}Al_{25}$	999	740		878	825

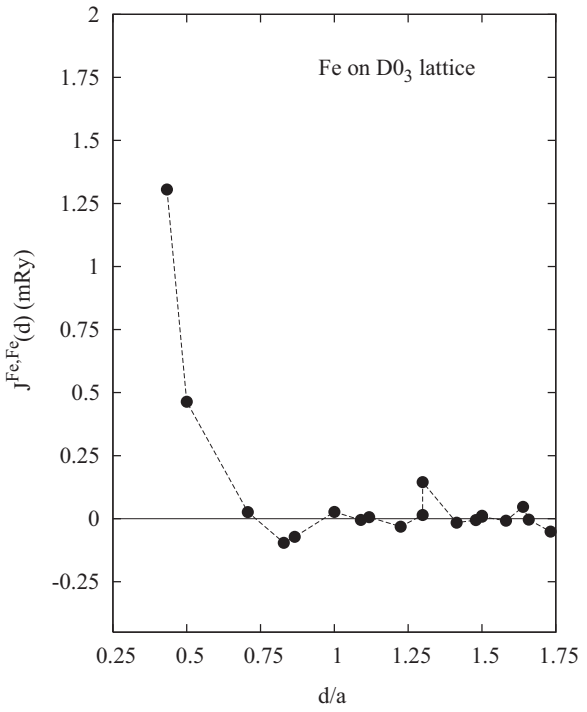

FIG. 3. The exchange interactions between Fe sites in the $D0_3$ structure for all sites occupied by iron with the formula Fe[A]-Fe[B]-Fe[C]-Fe[D] plotted as a function of the distance (d) in units of the lattice constant (a). The calculations were done for the lattice constant of Fe_3Si.

in Fig. 3. The dominating exchange interactions resemble an "envelope" of all Fe-Fe interactions found in Fe_3Si (see Fig. 2), although some differences for more distant shells can be found.

D. Curie temperatures

From calculated exchange integrals, we have estimated Curie temperatures (T_C) of Fe_3X (X = Al,Si) using the multisublattice versions of the MFA, RPA [17], and Monte Carlo (MC) methods. In the last case, we used the UPPASD package [30], which also contains the MC code with the METROPOLIS algorithm to estimate T_C. In all cases, we refer the interested reader to the above references for technical details. The results for various approximations are summarized in Table II together with experimental data.

The MFA overestimates the experimental values, as expected. However, the more important point is that the MFA fails to give a proper order of calculated T_C's observed in the experiment, namely $T_C[Fe_3Si] > T_C[Fe_3Al]$. On the other hand, both the RPA and MC simulations give a proper order of T_C's, although the calculated values are underestimated. This fact has to be ascribed to the behavior of Fe[A,C] moments mentioned above: the DLM moment of Fe[A,C] sites collapses to zero, as contrasted with the rigid moment on Fe[B] sites. The situation is similar to that known, e.g., in fcc Ni. The cure is to use the renormalized magnetic force theorem based on the constrained density functional theory as suggested in Refs. [31,32]. We employ here the approach of Bruno [31], called the renormalized RPA (rRPA), which allows for a simple generalization to a more complex systems. Recently, we have applied it successfully to random Ni-based fcc alloys [34]. It should be mentioned that theory based on the renormalized magnetic force theorem enhances the calculated Curie temperature. The rRPA Curie temperature (T_C^{rRPA}) is thus higher than the conventional RPA Curie temperature (T_C^{RPA}). Both T_C's are related using the calculated magnetic moment M and exchange splitting Δ due to the d electrons, which dominate the magnetic behavior of transition metals. In the present case, we use the effective moment M^{eff} and exchange splitting Δ^{eff} obtained by averaging over four sublattices. The result is

$$\left(k_B T_C^{rRPA}\right)^{-1} = \left(k_B T_C^{RPA}\right)^{-1} - \frac{6}{M^{eff}\Delta^{eff}}. \quad (6)$$

The renormalized value brings the theoretical estimate into better agreement with the experiment. It should be noted, however, that the above simple theory is just a step in the right direction. The multisublattice version of the rRPA method has been formulated [33] but not implemented yet.

At the end of this section, we discuss the MFA and RPA Curie temperatures in some detail. The dependence of Curie temperatures on the number of shells of exchange integrals expressed in terms of the cutoff distance is shown in Fig. 4. The MFA values are robust with respect to the cutoff distance, as contrasted with the RPA. This is particularly true for the Fe_3Al alloy showing rather large fluctuations of T^{RPA} with the cutoff distance. Both the MFA and RPA depend on the lattice Fourier transform $J(\mathbf{q})$ of the real-space exchange integrals J_{ij}, but values close to $q = 0$ are important for the RPA, which explains its sensitivity to the cutoff distance. In the numerical implementation of the multisublattice RPA [17], a damping parameter is introduced. This parameter somehow accounts for fluctuations caused by a finite cutoff distance and helps to stabilize T_C, especially for Fe_3Al. Corresponding error bars for the RPA are also shown in Table II . We note that exchange interactions for distances between $1.75a$ and $2.0a$ (a is the lattice constant) seem to be relevant for flipping the wrong order of T_C's of Fe_3Al and Fe_3Si.

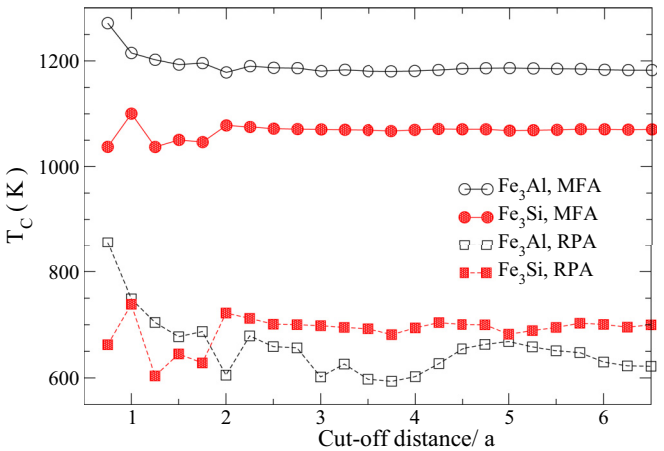

FIG. 4. (Color online) The MFA (circles) and RPA (squares) Curie temperatures as a function of the cutoff distance of exchange integrals included in calculations. The cutoff distance is in units of the lattice constant (a). Full and empty symbols correspond to Fe_3Si and Fe_3Al alloys, respectively.

The MC simulations are much more time-consuming, and we show in Table II just values for the cutoff radii $2a$ and $4a$. We observe the same trends, namely larger T_C of Fe_3Si as compared to Fe_3Al and the smaller sensitivity of T_C of Fe_3Si with respect to the shell number.

Finally, we also show in Table II the results for T_C of the related random bcc-$Fe_{75}Al_{25}$ alloy for which the experimental data exist in the literature [1]. The present results of MFA, RPA, and renormalized RPA [34] are shown, and the latter estimates agree reasonably well with the experiment. The higher T_C of the disordered phase than that of the ordered phase is due the different statistics of neighborhoods of Fe atoms: in the ordered phase, each atom Fe has on average 5.33 Fe nearest neighbors, while in the disordered phase it has on average 6 Fe nearest neighbors.

E. Sublattice magnetizations

We have also studied the temperature dependence of magnetization on the A/C and B sublattices. This study is motivated by Ref. [7], in which, using an empirical model employing the experimental data for the Fe hyperfine magnetic fields, it was shown that the relative sublattice magnetizations $m_\alpha = M_\alpha(T)/M_\alpha(T=0)$ plotted as a function of the relative temperature T/T_c are similar to each other (α = A/C or B). It is therefore interesting to test how this fact is reproduced by the present parameter-free theory. The temperature dependence of sublattice magnetizations was estimated from the Heisenberg Hamiltonian (2) using the UPPASD package [30]. In general, a different behavior is expected due to different exchange integrals reflecting the different environments of Fe[A,C] and Fe[B] atoms in both compounds (cf. Figs. 1 and 2). In the present study, we have concentrated on the Fe_3Si alloy, which exists in an almost perfect $D0_3$ structural phase.

The theoretical results for the relative sublattice magnetizations are shown in Fig. 5(a). We first mention two facts, namely (i) that the classical statistics used in the Monte Carlo simulation in the UPPASD package gives an incorrect linear decrease of magnetization for low temperatures (only the quantum statistics gives a correct Bloch's $T^{3/2}$ law [35]); and (ii) that due to finite-size effects (i.e., the finite size of the cell in Monte Carlo simulations), magnetizations do not sharply vanish at the Curie temperature (or at $T/T_c = 1$ in the present case). Calculated temperature dependences of relative magnetizations are similar despite their different environments, although quantitatively not so much as for the empirical model of Ref. [7] with parameters fitted to the experiment. This becomes clear if we plot the ratio of relative magnetizations $m_{A,C}$:m_B, which is shown as a dotted line in Fig. 5(a). This ratio should equal to 1 in the case when the T dependences of relative magnetizations are the same.

We demonstrate this point by showing in Fig. 5(b) the experimental results [36] for the relative hyperfine fields $h_\alpha(T) = H_\alpha(T)/H_\alpha(T=0)$, where H_α are measured sublattice hyperfine fields (α = A/C,B). Indeed, the ratio of relative hyperfine fields, $h_{A,C}$:h_B, is very close to 1. While the deviation of the ratio of relative magnetizations from 1 in Fig. 5(a) is partly due to the limitations of the present model discussed above, there are some general reasons why the relative hyperfine fields of different sublattices should exhibit smaller deviations than the corresponding relative magnetizations. In the Appendix, we present a simple model that attempts to explain the different behavior of sublattice magnetizations and hyperfine fields.

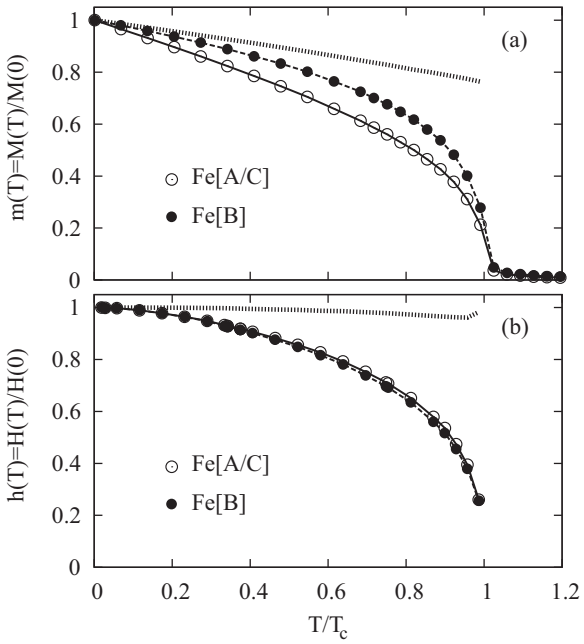

FIG. 5. (a) The relative sublattice magnetizations $m_\alpha(T) = M_\alpha(T)/M_\alpha(T=0)$ (α = A/C or B) plotted as a function of relative temperatures T/T_c for Fe_3Si (see text for definitions). Magnetizations are nonzero at $T/T_c = 1$ due to the finite-size effects close to T_c. The dotted line shows the ratio of relative sublattice magnetizations $m^{A/C}/m^B$. (b) The same but for relative sublattice hyperfine fields $h_\alpha(T) = H_\alpha(T)/H_\alpha(T=0)$ (α = A/C or B) as obtained from the experiment [36]. The dotted line shows the ratio of relative sublattice hyperfine fields $h^{A/C}/h^B$. The quantities $M(0)$ and $H(0)$ relate to $T = 0$.

F. Magnon spectra

Magnetic excitations and in particular magnon spectra can be accessed from atomistic spin dynamics (ASD) simulations. We refer the readers to Ref. [37] for all details needed to perform the ASD simulations including the temperature effect. The method can be applied in a first-principles mode, where all interatomic exchange interactions are calculated self-consistently, or, as in the present case, calculated for a fixed spin-configuration [parameters of the Heisenberg Hamiltonian (2)]. The dynamics at finite temperature are obtained in this method by solving the Landau-Lifshitz-Gilbert (LLG) equations for all atomic moments in the system. In particular, by calculating space and time averages of the correlation function of magnetic moments and performing its lattice Fourier transform, we obtain the dynamical structure factor $S(\mathbf{q},\omega)$, the quantity probed in neutron scattering experiments of bulk systems. Here, $\mathbf{q}$ and ω are the momentum and energy transfer, respectively. We obtain the magnon spectra by identifying the peak positions of $|S(\mathbf{q},\omega)|$ along particular directions in the reciprocal space. Due to the stochastic nature of simulations, the calculated $S(\mathbf{q},\omega)$ spectra are typically very

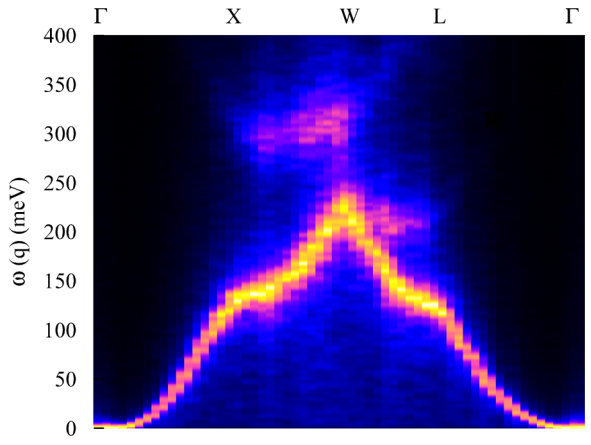

FIG. 6. (Color online) Calculated magnon dispersion of Fe_3Al at $T = 300$ K.

diffuse. The identification of peaks is not a simple task, and one has to use specific schemes to overcome this problem (see Ref. [38] and references there). In the present study, we consider the broadening of the magnon dispersion due to the transversal temperature fluctuations of the magnetic moments originating from the coupled thermal bath. We neglect the damping due to the longitudinal Stoner excitations.

For $\mathbf{q}$ vectors close to the Γ point in the Brillouin zone, the magnon energy $\omega(\mathbf{q})$ for the cubic system has a quadratic dependence on $\mathbf{q}$, i.e., $\omega(\mathbf{q}) = Dq^2$, where D is the spin-wave stiffness and $q = |\mathbf{q}|$. The calculated magnon dispersions at room temperature of Fe_3Al and Fe_3Si, respectively, are displayed in Figs. 6 and 7. The maximum peak value is marked by yellow in the plots. The damping parameter α in the LLG equations [37] was set to 0.05, but the spectra should not be too sensitive to it. Overall, the magnon spectra are slightly softer for Fe_3Al than for Fe_3Si, which is consistent with the lower Curie temperature found for Fe_3Al. Because the spin stiffness is the curvature of the magnon dispersion in the limit $\mathbf{q} \to \mathbf{0}$, one can conclude from Figs. 6 and 7 that the spin stiffness is lower in Fe_3Al as compared to Fe_3Si.

The evaluation of the spin stiffness D is a delicate task [16]. We have determined D's using the frozen magnon approach

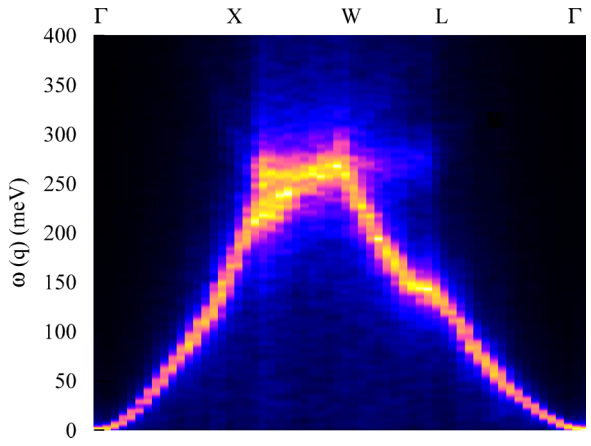

FIG. 7. (Color online) Calculated magnon dispersion of Fe_3Si at $T = 300$ K.

in which the lattice Fourier transform of calculated exchange integrals up to a distance of four lattice constants is fitted to Dq^2 for small $\mathbf{q}$ values ($q < 0.3$ Å^{-1}) in the Γ-X direction in the Brillouin zone. Since a very dense grid can be employed, such fitting is much more reliable as compared to the corresponding fit based on magnon spectra in Figs. 6 and 7, which were calculated using the ASD on a relatively sparse grid. Calculated spin stiffnesses for Fe_3Si and Fe_3Al are, respectively, 207 and 130 meV Å^2. Experimental values of the spin stiffness for Fe_3Si are 145 ± 1 meV Å^2, Ref. [39], and 158 ± 2 meV Å^2, Ref. [40], respectively. On the other hand, a larger dispersion of measured values of spin stiffnesses exists for Fe_3Al, namely 83 ± 4 meV Å^2, Ref. [41], and 139 ± 6 meV Å^2 in a more recent study [42]. One can conclude that experimental and calculated values are in an acceptable agreement, and, in particular, the larger spin stiffness of Fe_3Si is reproduced.

G. Transport properties

In this section, we complete the study of various properties of Fe_3X alloys by adding the results of transport studies. The experimental values of the total residual resistivity ρ_{tot} at $T = 0$ K are around 5 $\mu\Omega$ cm for Fe_3Si and 30 $\mu\Omega$ cm for Fe_3Al [43]. This illustrates the fact that Fe_3Si alloys can be prepared in a form close to the ideal $D0_3$ structure. For example, for slowly cooled down Fe_3Si specimens, the authors of Ref. [44] report very low resistivity (0.6 $\mu\Omega$ cm), indicating an almost perfect stoichiometric $D0_3$ crystal. On the other hand, a much larger value of ρ_{tot} in the Fe_3Al is present due to the native disorder in this compound, illustrating the fact that the Fe_3Al is much more difficult to prepare as an ideal crystal. A detailed analysis of the disorder in Fe_3Al was done in Ref. [45]. The corresponding structural model, in terms of sublattice disorder, is (Fe_{97},Al_3)-(Fe_{98},Al_2)-(Fe_{97},Al_3)-(Al_{92},Fe_8) for Fe_3Al. We remark that in this notation, the ideal Fe_3Al has the sublattice order Fe-Fe-Fe-Al. No such study exists for Fe_3Si with a much weaker native disorder. We have therefore tested a few cases with small Si[Fe] antisite concentrations x, corresponding to the structural model $(Fe_{1-x},Si_x)_3(Si_{1-3x},Fe_{3x})$.

The resistivities of Fe_3Al and Fe_3Si were calculated using the KG approach and assuming the same lattice constants as in the ideal samples. We have obtained $\rho_{\text{tot}} = 32.1$ $\mu\Omega$ cm by adopting the structural model of Ref. [45] for Fe_3Al, in good agreement with the experiment. Assuming small antisite concentrations $x_{\text{Si[Fe]}}$ equal to 0.2% (0.5%), we obtained $\rho_{\text{tot}} = 5.6$ (13.2) $\mu\Omega$ cm, respectively. We observe an almost linear increase of ρ_{tot} in Fe_3Si with the antisite concentration. The lower value of ρ_{tot} for Fe_3Si also agrees well with the experiment.

Below we discuss in detail the transport calculations. Specifically, the coherent parts ρ_{coh} of total resistivities ρ_{tot}, i.e., the values neglecting the disorder-induced vertex parts, are 40.4 and 5.9 $\mu\Omega$ cm for Fe_3Al and Fe_3Si (with $x_{\text{Si[Fe]}} = 0.2\%$), respectively. In other words, the vertex part contributes by about 26% (5%) for Fe_3Al (Fe_3Si), respectively. In the present scalar-relativistic calculations, it is possible to separate out the contributions of different spin channels. The results are summarized in Table III, where also vertex corrections are given. We note a different ratio of spin-resolved conductivities

TABLE III. The calculated total and spin-resolved conductivities [in atomic units $e^2/(ha_0)$, where a_0 is the Bohr radius] for Fe_3Si and Fe_3Al. The vertex parts of the conductivities are also given.

Alloy	$\sigma_{tot}^{\uparrow}$	$\sigma_{tot}^{\downarrow}$	σ_{tot}	$\sigma_{vtx}^{\uparrow}$	$\sigma_{vtx}^{\downarrow}$	σ_{vtx}
Fe_3Si	5.08	7.14	12.22	0.76	−0.16	0.60
Fe_3Al	1.57	0.55	2.12	0.42	0.02	0.44

and even negative vertex corrections for the spin-down channel in Fe_3Si, which was also found for $x_{Si[Fe]} = 0.5\%$. Such unusual behavior as compared to alloys on simple lattices is due to the different effect of antisite disorder on different sublattices and also to the different band fillings (Fe_3Si has one more valence electron than Fe_3Al) and thus also different Fermi surfaces.

IV. CONCLUSIONS

We have presented, based on the unified first-principles model, estimates of a broad range of physical properties of Fe_3X (X = Al,Si) alloys with $D0_3$ structure. There is good agreement between the present theory, existing theoretical approaches, and experiment for the total and sublattice magnetic moments. The main results are as follows: (i) Using Fe_3Al as a case study, we have shown that the $D0_3$ lattice develops from the disordered bcc-phase on cooling in two steps. The first ordering is into the intermediate B2 type structure, and from it, after further cooling, the second ordering into the final $D0_3$ structure occurs in agreement with the experiment. We have found that the presence of magnetic moments is important, especially for the second ordering. The order of structure ordering temperatures, estimated using the mean-field concentration-wave method, is correct, but their values are overestimated. Similar results were obtained also for Fe_3Si. Theory correctly predicts a much larger ordering temperature of Fe_3Si as compared to Fe_3Al. (ii) The MFA overestimates Curie temperatures and gives their wrong order for Fe_3Al and Fe_3Si. The RPA gives a correct order of Curie temperatures, but it underestimates them. The most likely reason are soft moments of Fe atoms on A and C sublattices that collapse during rotations in the spin subspace. We have shown that the renormalized RPA approach accounts for this fact and brings theoretical results into reasonable agreement with the experiment. (iii) The relative sublattice magnetizations exhibit slightly different temperature dependences due to the different exchange interactions. Based on a simple model, we have explained that this result does not contradict the experimentally observed temperature dependences of hyperfine fields, which are nearly identical for all Fe sublattices. (iv) The calculated spin stiffnesses agree reasonably well with experimental data; their values for Fe_3Si are larger than values for Fe_3Al. (v) We have estimated the resistivity at low temperatures using the KG approach. The relatively large residual resistivity of Fe_3Al found in the experiment was reproduced using the model of structural disorder. The experimental value of residual resistivity of Fe_3Si was reproduced assuming a substantially smaller Fe-Si swapping disorder.

ACKNOWLEDGMENTS

J.K., V.D., and I.T. acknowledge the support of the Czech Science Foundation (Grant No. P204/12/0692) and the Czech-Hungarian collaboration. J.R. acknowledges the Swedish Research Council and the EU project REFREEPERMAG. L.B. acknowledges support from the Swedish Research Council (VR), Göran Gustafsson Foundation, Carl Tryggers Foundation, and SeRC. B.U. and I.V. acknowledge support from the Hungarian Scientific Research Fund (OTKA) through Grants No. 84078 and No. 101456, respectively.

APPENDIX: RELATION BETWEEN LOCAL MOMENTS AND HYPERFINE FIELDS

The different temperature dependences of the reduced (relative) sublattice magnetizations as calculated using the present approach (Fig. 5) reflect directly the differences in the exchange interactions among the local Fe moments (Figs. 1 and 2). On the other hand, the experimentally accessible hyperfine fields at iron nuclei often exhibit temperature dependences that are nearly identical for all sublattices [7]. Since the hyperfine fields in iron alloys are closely related to the magnetic moments, we sketch here an explanation of this seeming contradiction in terms of a simple model. The essential feature of our model is to provide different values of sublattice magnetizations as independent variables, which, however, lead to very similar values of the hyperfine magnetic fields. Such a model can be formulated, e.g., in terms of an uncompensated collinear disordered-local-moment (DLM) model (see below).

Our starting point is a semiempirical linear relation [7] between the sublattice-resolved hyperfine fields $H_\alpha(T)$ and the local moments $M_\alpha(T)$, namely,

$$H_\alpha(T) = \sum_\beta W_{\alpha\beta} M_\beta(T), \tag{A1}$$

where the subscripts $\alpha,\beta \in \{\mathrm{A},\mathrm{B}\}$ denote the two inequivalent iron sublattices (A ≡ C) and the coefficients $W_{\alpha\beta}$ are temperature-independent constants. A similar linear relation between the reduced quantities, $h_\alpha(T) = H_\alpha(T)/H_\alpha(0)$ and $m_\alpha(T) = M_\alpha(T)/M_\alpha(0)$, can be written as

$$h_\alpha(T) = \sum_\beta w_{\alpha\beta} m_\beta(T), \tag{A2}$$

where the new coefficients are defined as $w_{\alpha\beta} = H_\alpha^{-1}(0) W_{\alpha\beta} M_\beta(0)$. They satisfy the obvious conditions

$$\sum_\beta w_{\alpha\beta} = 1, \tag{A3}$$

valid for each α.

If all coefficients $W_{\alpha\beta}$ in (A1) and all sublattice magnetizations $M_\alpha(0)$ are positive, then the resulting coefficients $w_{\alpha\beta}$ are positive as well and they can be interpreted as weights normalized to unity due to the condition (A3). The reduced hyperfine fields $h_\alpha(T)$ are then weighted averages of the reduced magnetizations $m_\beta(T)$, see Eq. (A2), which means that both values $h_\mathrm{A}(T)$ and $h_\mathrm{B}(T)$ fall inside the interval bounded by the values $m_\mathrm{A}(T)$ and $m_\mathrm{B}(T)$. Consequently,

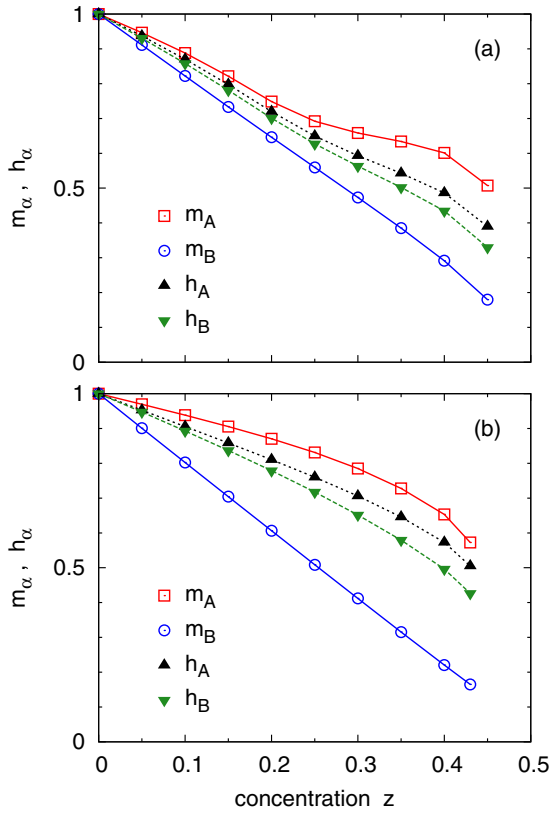

FIG. 8. (Color online) The concentration dependence of the reduced sublattice-resolved hyperfine fields, $h_\alpha(z)$, and magnetizations, $m_\alpha(z)$, in the DLM model on the Fe[B] sublattice: (a) for the Fe_3Si compound and (b) for the Fe_3Al compound.

$|h_A(T) - h_B(T)| \leqslant |m_A(T) - m_B(T)|$, and the two reduced hyperfine fields are in general closer to each other than the two reduced magnetic moments. This analysis, based on the linear relation (A1), indicates that the above-mentioned different temperature dependences of the reduced magnetizations can be compatible with very similar temperature trends of the reduced hyperfine fields.

The physical justification for the semiempirical relation (A1) rests on the well-known mechanisms of the hyperfine fields, including both local (core polarization) and nonlocal (transferred fields) contributions. Nevertheless, its accuracy as well as the positivity of all coefficients $W_{\alpha\beta}$ have to be checked for each particular system. In the present case of Fe_3X (X = Si,Al) compounds, we have introduced a concentration variable z ($0 \leqslant z < 0.5$) that defines the orientation of the Fe[B] moments as a random binary alloy $Fe^+_{1-z}Fe^-_z$, where Fe^+ and Fe^- denote iron atoms with positive and negative moments, respectively (the uncompensated DLM model on the Fe[B] sublattice). We have employed the nonrelativistic version of the TB-LMTO-CPA method with an *spd* basis set and with the limitation of the hyperfine fields to the Fermi contact term (proportional to the spin density at the pointlike Fe nucleus). In such a theory, the hyperfine fields and magnetic moments on the Fe[B] sublattice are obtained as concentration-weighted averages of the quantities for Fe^+ and Fe^- atomic species. Consequently, the scan over the concentration from $z = 0$ up to the vicinity of $z = 0.5$ mimics the reduction of the average alloy magnetization between zero temperature and the Curie point.

The least-squares fitting of the calculated fields $H_\alpha(z)$, based on the linear relation in analogy to (A1), i.e., $H_\alpha(z) = \sum_\beta W_{\alpha\beta} M_\beta(z)$, results in a good accuracy of the fits and in positive signs of all coefficients $W_{\alpha\beta}$. This confirms the validity of the above analysis for the studied systems. Moreover, the concentration dependences of the calculated reduced (relative) sublattice-resolved fields, $h_\alpha(z) = H_\alpha(z)/H_\alpha(0)$, and moments, $m_\alpha(z) = M_\alpha(z)/M_\alpha(0)$, plotted in Fig. 8 for both studied compounds, prove explicitly that the differences in the reduced fields are substantially smaller as compared to the differences in the reduced magnetizations. Note that the magnetization on the B sublattice is smaller as compared to the A (C) sublattice, which contradicts the real temperature dependences discussed in Sec. III E. This fact points to the true merit of the introduced DLM model, which has been designed merely as a tool for a quantitative analysis of the relation between the local magnetizations and the hyperfine fields, whereas further aspects of the finite-temperature behavior cannot be treated within this simple framework.

[1] O. Kubaschewski, *Iron-Binary Phase Diagrams* (Springer, Berlin, 1982).
[2] T. J. Burch, T. Litrenta, and J. I. Budnick, Phys. Rev. Lett. **33**, 421 (1974).
[3] J. Y. Rhee and B. N. Harmon, Phys. Rev. B **70**, 094411 (2004).
[4] N. E. Christensen, J. Kudrnovský, and C. O. Rodriguez, Int. J. Nanoelectron. Mater. **1**, 1 (2008).
[5] A. C. Switendick, Solid State Commun. **19**, 511 (1976).
[6] S. Ishida, I. Ishida, S. Asano, and J. Yamashita, J. Phys. Soc. Jpn. **41**, 1570 (1976).
[7] M. B. Stearns, Phys. Rev. **168**, 588 (1968).
[8] O. K. Andersen and O. Jepsen, Phys. Rev. Lett. **53**, 2571 (1984).
[9] S. H. Vosko, L. Wilk, and M. Nusair, Can. J. Phys. **58**, 1200 (1980).
[10] I. Turek, V. Drchal, J. Kudrnovský, M. Šob, and P. Weinberger, *Electronic Structure of Disordered Alloys, Surfaces and Interfaces* (Kluwer, Boston, 1997); I. Turek, J. Kudrnovský, and V. Drchal, in *Electronic Structure and Physical Properties of Solids*, edited by H. Dreyssé, Lecture Notes in Physics Vol. 535 (Springer, Berlin, 2000), p. 349.
[11] F. Ducastelle, *Order and Phase Stability in Alloys* (North-Holland, Amsterdam, 1991).
[12] J. Kudrnovský, I. Turek, A. Pasturel, R. Tetot, V. Drchal, and P. Weinberger, Phys. Rev. B **50**, 9603 (1994).
[13] J. W. D. Connolly and A. R. Williams, Phys. Rev. B **27**, 5169 (1983).
[14] A. I. Liechtenstein, M. I. Katsnelson, V. P. Antropov, and V. A. Gubanov, J. Magn. Magn. Mater. **67**, 65 (1987).

[15] I. Turek, J. Kudrnovský, V. Drchal, and P. Bruno, Philos. Mag. **86**, 1713 (2006).
[16] M. Pajda, J. Kudrnovský, I. Turek, V. Drchal, and P. Bruno, Phys. Rev. B **64**, 174402 (2001).
[17] J. Rusz, I. Turek, and M. Diviš, Phys. Rev. B **71**, 174408 (2005).
[18] I. Turek, J. Kudrnovský, V. Drchal, L. Szunyogh, and P. Weinberger, Phys. Rev. B **65**, 125101 (2002).
[19] K. Carva, I. Turek, J. Kudrnovský, and O. Bengone, Phys. Rev. B **73**, 144421 (2006).
[20] J. C. Swihart, W. H. Butler, G. M. Stocks, D. M. Nicholson, and R. C. Ward, Phys. Rev. Lett. **57**, 1181 (1986).
[21] The DLM state corresponds to the magnetic state with spins oriented randomly in each direction with the same probability and with the zero total moment. The problem can be formally mapped onto the random equiconcentration alloy with spins pointing up and down, and corresponding self-consistent magnetic moments can thus be determined using the CPA. For details, see B. L. Gyorffy, A. J. Pindor, J. Staunton, G. M. Stocks, and H. Winter, J. Phys. F **15**, 1337 (1985).
[22] The corrections for the temperature dependence of the magnetic moments were taken from the present hyperfine field data, which are in accord with the magnetization measurements in the measured temperature range of 5–300 K. The present samples are not necessarily identical with those used in the neutron diffraction measurements, Refs. [23–25] e.g., the composition or the state of the order may be slightly different. The errors caused by these possible differences are small compared to the error of the neutron diffraction measurements due to finite temperature and to the magnitude of corrections. It should be noted that values measured at room temperature are about 10% smaller as compared to the corrected ones corresponding to the temperature of 5 K so that corrections are not negligible.
[23] A. Paoletti and L. Passari, Il Nuovo Cimento **32**, 25 (1964).
[24] J. Moss and P. J. Brown, J. Phys. F **2**, 358 (1972).
[25] S. J. Pickart and R. Nathans, Phys. Rev. **123**, 1163 (1961).
[26] F. Lechermann, F. Welsch, C. Elsässer, C. Ederer, M. Fähnle, J. M. Sanchez, and B. Meyer, Phys. Rev. B **65**, 132104 (2002).
[27] S. Dennler and J. Hafner, Phys. Rev. B **73**, 174303 (2006).
[28] D. G. Morris and S. Gunther, Acta Mater. **44**, 2847 (1996).
[29] A. V. Ruban, S. I. Simak, P. A. Korzhavyi, and H. L. Skriver, Phys. Rev. B **66**, 024202 (2002).
[30] Uppsala Atomistic Spin Dynamics Project, URL: http://www.physics.uu.se/en/pages/UppASD.
[31] P. Bruno, Phys. Rev. Lett. **90**, 087205 (2003).
[32] V. I. Antropov, J. Magn. Magn. Mater. **262**, L192 (2003).
[33] J. Rusz, Ph.D. thesis, Charles University, Prague, 2005.
[34] J. Kudrnovský, V. Drchal, and P. Bruno, Phys. Rev. B **77**, 224422 (2008).
[35] N. W. Ashcroft and N. D. Mermin, *Solid State Physics* (Holt, Rinehart and Winston, New York, 1976), pp. 708–709.
[36] I. Vincze (unpublished results). Very similar results were reported earlier (although for a smaller number of relative temperatures) by Stearns [7].
[37] B. Skubic, J. Hellsvik, L. Nordström, and O. Eriksson, J. Phys.: Condens. Matter **20**, 315203 (2008).
[38] A. Bergman, A. Taroni, L. Bergqvist, J. Hellsvik, B. Hjörvarsson, and O. Eriksson, Phys. Rev. B **81**, 144416 (2010).
[39] L. Dobrzyński, A. Wiśniewski, Y. J. Uemura, S. M. Shapiro, and J. P. Wicksted, Phys. Rev. B **37**, 7175 (1988).
[40] G. Parzych, J. Jankowska-Kisielinska, and L. Dobrzyński, Acta Phys. Pol. A **117**, 578 (2010).
[41] B. Antonini, F. Menzinger, and A. Paoletti, J. Phys. (Paris) Colloq. **32**, C1-1188 (1971).
[42] E. Frikkee, J. Phys. F **8**, L141 (1978).
[43] W. B. Muir, J. I. Budnick, and K. Raj, Phys. Rev. B **25**, 726 (1982).
[44] J. B. Raush and F. X. Kayser, J. Appl. Phys. **48**, 487 (1977).
[45] A. J. Bradley and A. H. Jay, Proc. R. Soc. London, Ser. A **136**, 210 (1932).
[46] Y. Nakayama, in *Landolt-Börnstein*, Ser. III, Vol. 19c, Part 2 (Springer, Berlin, 1988).